heavy atoms, a difference-Fourier map revealed maxima of residual electronic density close to the positions expected for hydrogen atoms of the porphyrin and the tosyl group; they were introduced in structure factor calculations by their computed coordinates (C-H = 0.95 Å) and isotropic temperature factors of $B(H) = 1 + B_{eq}(C)$ Å^2 but not refined. CH_3OH and water hydrogens were omitted. Full least-squares refinement minimizing $\sum w(|F_o| - |F_c|)^2$ converged to $R(F) = 0.058$ and $R_w(F) = 0.087$ with $\sum w(F^2) = (\sigma^2(\text{counts}) + (pI)^2)^{-1}$. The unit-weight observation was 1.73 for $p = 0.08$. A final difference map revealed no significant maxima. The scattering factor coefficients and anomalous dispersion coefficients come respectively from ref 36 and 37.

Table IV gives the X-ray coordinates of each atom of complex **2a**.

Reagents and Solvents. Methylene chloride was purified by distillation from P_2O_5 and kept over molecular sieves. Pentane and methanol for crystallization were used as supplied by Prolabo (purissimum grade) [(tosylimino)iodo]benzene, PhI=NTs (**1**), was synthesized according to an already described procedure[17] and stored at 0 °C, in the dark, under argon to avoid decomposition. Fe(TPP)(Cl), Fe(TTP)(Cl), and Fe(TpClPP)(Cl) were prepared according to literature procedures.[38,39]

Synthesis of Complexes 2a-c: Tosylimido-Bridged Iron(III) *meso*-Tetraphenylporphyrin Chloride, Fe^{III}(TPP)(NTs)(Cl) (2a). A solution of 0.07 g of Fe^{III}(TPP)(Cl) in 10 mL of CH_2Cl_2 at 20 °C was added under argon to 0.15 g of solid PhI=NTs, in the presence of molecular sieves. After 15 min of stirring, the formation of complex **2a** was complete. The solution was then filtered, and complex **2a** precipitated as a red-brown powder with ca. 20 mL of pentane. Purple shining cristals of **2a** were obtained with a 80% yield (0.07 g) after recrystallization from CH_2Cl_2-CH_3OH (2:1). Anal. Calcd for $C_{51}H_{35}N_5O_2SFeCl$: C, 70.15; H, 4.04; N, 8.02; S, 3.67; Cl, 4.06. Found: C, 69.94; H, 4.24; N, 8.20; S, 3.62; Cl, 3.87.

Tosylimido-Bridged Iron(III) *meso*-Tetrakis(*p*-chlorophenyl)porphyrin Chloride, Fe^{III}(TpClPP)(NTs)(Cl) (2b). **2b** was prepared as described above, by starting from 0.084 g of Fe^{III}(TpClPP)(Cl) and 0.15 g of PhI=NTs (0.096 g, yield 95%). Anal. Calcd for $C_{51}H_{31}N_5SO_2Cl_5Fe$: C, 60.59; H, 3.09; N, 6.92; S, 3.17. Found: C, 60.45; H, 3.36; N, 6.30; S, 3.45.

Tosylimido-Bridged Iron(III) *meso*-Tetra-*p*-tolylporphyrin Chloride Fe^{III}(TTP)(NTs)(Cl) (2c). **2c** was prepared by starting from 0.076 g of Fe^{III}(TTP)(Cl) and 0.15 g of PhI=NTs (0.083 g, yield 90%). Anal. Calcd for $C_{55}H_{43}N_5SO_2ClFe$: C, 71.09; H, 4.66; N, 7.54; S, 3.45. Found: C, 70.92; H, 4.89; N, 7.80; S, 3.61.

The other characteristics of complexes **2a-c** (mass, UV-vis, ^{1}H NMR, and IR spectral data) are included in the tables.

Registry No. **1**, 55962-05-5; **2a**, 111468-47-4; **2b**, 111468-48-5; **2c**, 111468-49-6; Fe(TPP)(Cl), 16456-81-8; Fe(TpClPP)(Cl), 36965-70-5; Fe(TTP)(Cl), 19496-18-5; Fe(TPP)(NTS)(Br), 111468-50-9; Fe(TPP)(Br), 25482-27-3.

Supplementary Material Available: Thermal parameters (U_{ij}) for all anisotropic atoms (Table V), positional parameters for hydrogen atoms (Table VI), a full set of bond lengths (Table VII), and a full set of bond angles (Table VIII) (8 pages); observed and calculated structure factor amplitudes (×10) for all observed reflections (Table IX) (16 pages). Ordering information is given on any current masthead page.

(36) Cromer, D. T.; Waber, J. T. *International Tables for X-ray Crystallography*; Kynoch: Birmingham, England, 1974; Vol. IV, Table 2-2b.
(37) Cromer, D. T.; Waber, J. T. *International Tables for X-ray Crystallography*; Kynoch: Birmingham, England, 1974, Vol. IV; Table 2.3.1.
(38) (a) Barnet, G. H.; Hudson, M. F.; Smith, K. M. *Tetrahedron Lett.* **1973**, *30*, 2887-2888. (b) Adler, A. D.; Longo, F. R.; Kampas, F.; Kim. J. *J. Inorg. Nucl. Chem.* **1970**, *32*, 2443-2445.
(39) Fuhrop, J. H.; Smith, K. M. In *Porphyrins and Metalloporphyrins*; Smith, K. M., Ed.; Elsevier: Amsterdam, 1975; pp 769-774.

Contribution from the USDA/ARS Western Regional Research Center, Albany, California 94710, and Department of Chemistry, Florida Atlantic University, Boca Raton, Florida 33431

Correlation of Redox and Spectroscopic Properties in Seven-Coordinate Oxomolybdenum(VI) Hydroxylamido Catecholato Complexes

Stephen F. Gheller,[1a] William E. Newton,*[1a] Ligia Pabon de Majid,[1b,c] Julie R. Bradbury,[1b,d] and Franklin A. Schultz*[1b,e]

Received May 28, 1987

Seven-coordinate $MoO(cat)(ONR_2)_2$ complexes (R = Me, Et, Bz) are prepared by reaction of *cis*-$MoO_2(ONR_2)_2$ with catechol and its 4-nitro, 4-methyl, and 3,5-di-*tert*-butyl derivatives. Correlations among the electrochemical and IR, UV-visible, and ^{95}Mo NMR spectroscopic properties of these compounds are reported and contrasted with the behavior of compositionally similar $MoO(cat)(S_2CNEt_2)_2$ species. Both series of complexes undergo Mo-centered reductions and catechol-centered oxidations and exhibit an intense, visible wavelength absorption band that is assigned to cat → Mo charge transfer. Linear correlations exist between the difference in Mo- and catechol-centered redox potentials (ΔE_{redox}) and the energy ($h\nu_{ct}$) of the LMCT; however, values of ΔE_{redox} and $h\nu_{ct}$ are consistently larger for $MoO(cat)(ONR_2)_2$. This result implies that R_2NO^- interacts more strongly than $Et_2NCS_2^-$ with the $[MoO(cat)]^{2+}$ center, thus producing a greater separation between the filled catecholate and vacant Mo orbitals involved in the electrochemical and spectroscopic transitions. The $MoO(cat)(ONR_2)_2$ (R = Me, Et) complexes exhibit a ^{95}Mo NMR chemical shift that correlates linearly with the wavelength of the LMCT in accord with shielding theory for heavy nuclei. A secondary correlation exists between $\delta(^{95}Mo)$ and the Mo-centered reduction potentials, apparently as a result of the relationship between electrochemical and optical properties. Solid-state FT/IR spectra of the 4-nitro and 3,5-di-*tert*-butyl derivatives of $MoO(cat)(ONR_2)_2$ show two Mo=O stretching frequencies between 915 and 930 cm^{-1}. These are attributed to the two geometric isomers that become possible when an unsymmetrically substituted catechol ligand is bound to $[MoO(ONR_2)_2]^{2+}$.

Introduction

Interest in oxomolybdenum compounds derives, in part, from the presence of this functionality at the active site of molybdenum hydroxylase enzymes.[2] Discovery of a pterin ring in the cofactor of these enzymes[3] raises the possibility that this organic unit may participate in electron transfer with the metal center, possibly during catalysis. Thus, we have become interested in oxomolybdenum complexes with redox-active ligands. Recently, we described[4] the preparation and electrochemical characterization of a series of oxomolybdenum(VI)-catecholate complexes with

(1) (a) USDA/ARS Western Regional Research Center. (b) Florida Atlantic University. (c) NSF Research Opportunity Award participant from the Department of Chemistry, University of Cayey, Cayey, PR 00633. (d) Present address: Department of Chemistry, Washington University, St. Louis, MO 63130. (e) Present address: Department of Chemistry, Indiana University-Purdue University at Indianapolis, Indianapolis, IN 46223.
(2) (a) Garner, C. D.; Bristow, S. In *Molybdenum Enzymes*, Spiro, T. G., Ed.; Wiley: New York, 1985; Chapter 7. (b) Holm, R. H.; Berg, J. M. *Pure Appl. Chem.* **1984**, *56*, 1645. (c) Spence, J. T. *Coord. Chem. Rev.* **1983**, *48*, 59. (d) Bray, R. C. In *The Enzymes*; Boyer, P. D., Ed.; Academic: New York, 1975; Vol. 12, Chapter 6.
(3) (a) Johnson, J. L.; Hainline, B. E.; Rajagopalan, K. V.; Arison, B. H. *J. Biol. Chem.* **1984**, *259*, 5414. (b) Johnson, J. L.; Rajagopalan, K. V. *Proc. Natl. Acad. Sci. U.S.A.* **1982**, *79*, 6856. (c) Cramer, S. P.; Stiefel, E. I. In *Molybdenum Enzymes*; Spiro, T. G., Ed.; Wiley: New York, 1985; Chapter 8.
(4) (a) Bradbury, J. R.; Schultz, F. A. *Inorg. Chem.* **1986**, *25*, 4408. (b) Bradbury, J. R.; Schultz, F. A. *Inorg. Chem.* **1986**, *25*, 4416. (c) Schultz, F. A. *J. Electroanal. Chem. Interfacial Electrochem.* **1986**, *213*, 167.

0020-1669/88/1327-0359$01.50/0

Table I. Analytical and Spectroscopic Data for $MoO(X\text{-}cat)(ONR_2)_2$ Complexes

(a) Analytical Data

	yield, %	anal. calcd, % (found, %) C	H	N
$MoO(NO_2cat)(ONMe_2)_2$	90	31.18 (31.31)	3.93 (3.95)	10.91 (10.79)
$MoO(Cat)(ONMe_2)_2$	59	35.29 (34.83)	4.74 (4.98)	8.22 (8.38)
$MoO(CH_3cat)(ONMe_2)_2$	44	37.30 (37.25)	5.12 (5.20)	7.91 (7.70)
$MoO(DTBcat)(ONMe_2)_2$	52	47.79 (47.90)	7.13 (7.52)	6.19 (6.26)
$MoO(NO_2cat)(ONEt_2)_2$	65	38.11 (38.40)	5.25 (5.88)	9.52 (9.69)
$MoO(Cat)(ONEt_2)_2$	86	42.43 (42.28)	6.10 (6.26)	7.07 (7.08)
$MoO(CH_3cat)(ONEt_2)_2$	74	43.91 (43.62)	6.39 (6.59)	6.83 (6.79)
$MoO(DTBcat)(ONEt_2)_2$	94	51.96 (51.57)	7.93 (8.06)	5.51 (5.42)
$MoO(NO_2cat)(ONBz_2)_2$	84	59.22 (59.90)	4.53 (4.84)	6.09 (5.70)
$MoO(Cat)(ONBz_2)_2$	85	63.36 (63.76)	5.00 (5.17)	4.35 (4.35)
$MoO(CH_3cat)(ONBz_2)_2$	83	63.83 (60.10)	5.20 (5.30)	4.25 (4.68)
$MoO(DTBcat)(ONBz_2)_2$	86	66.66 (64.00)	6.39 (6.36)	3.70 (3.73)

(b) Spectroscopic Data

	UV-vis[a] λ_{max}, nm (ϵ, M^{-1} cm^{-1})			IR ν(Mo=O), cm^{-1}	^{95}Mo NMR[a] δ	fwhm, Hz
$MoO(NO_2cat)(ONMe_2)_2$	460 (6390)	371 (7150)	303 (7300)	929 sh, 922	−55	200
$MoO(Cat)(ONMe_2)_2$	503 (4170)	304 (2870)	283 (3380)	926	−20	320
$MoO(CH_3cat)(ONMe_2)_2$	518 (4710)	313 sh (2920)	290 (3570)	926	−4	130
$MoO(DTBcat)(ONMe_2)_2$	528 (4810)	318 (2680)		921, 913	5	170
$MoO(NO_2cat)(ONEt_2)_2$	457 (5310)	374 (6100)	304 (6100)	931	−36	320
$MoO(Cat)(ONEt_2)_2$	500 (3950)	312 sh (2980)	280 (4290)	924	0	290
$MoO(CH_3cat)(ONEt_2)_2$	516 (4670)	318 sh (3100)	290 (3970)	924	12	310
$MoO(DTBcat)(ONEt_2)_2$	528 (5120)	316 (3140)		924, 915	19	410
$MoO(NO_2cat)(ONBz_2)_2$	471 (3750)	361 (4820)		[c]	[d]	
$MoO(Cat)(ONBz_2)_2$	514[b]	304	285 sh	926	[d]	
$MoO(CH_3cat)(ONBz_2)_2$	529[b]	308 sh		923	[d]	
$MoO(DTBcat)(ONBz_2)_2$	542[b]	321		923, 916 sh	[d]	

[a] In MeCN. [b] Insufficiently soluble for accurate determination of ϵ. [c] No assignment made; see text for discussion. [d] Insufficiently soluble for definitive assignment.

dithiocarbamate coligands, $MoO(cat)(S_2CNEt_2)_2$, that undergo both metal- and (catechol) ligand-centered electron-transfer reactions. This paper concerns a series of complexes with hydroxylamido coligands, $MoO(cat)(ONR_2)_2$, where cat^{2-} = the catecholate dianion or its 4-nitro (NO_2cat^{2-}), 4-methyl (CH_3cat^{2-}), or 3,5-di-*tert*-butyl ($DTBcat^{2-}$) derivative, and R = CH_3, C_2H_5, or $C_6H_5CH_2$. Related compounds with the 1-piperidinolate ($C_5H_{10}NO^-$) coligand have been prepared; the $MoO(cat)(ONC_5H_{10})_2$ member of this series has been characterized structurally and found to have a seven-coordinate pentagonal-bipyramid geometry.[5] Herein, we describe preparation of the hydroxylamido complexes, correlations among their electrochemical, infrared, electronic and ^{95}Mo NMR spectral properties and a comparison with results for the $MoO(cat)(S_2CNEt_2)_2$ complexes. Of interest is the manner in which the redox and spectroscopic properties of $MoO(cat)(L\text{-}L)_2$ respond to changes in molecular structure involving either an alteration of the L-L coligand from $Et_2NCS_2^-$ to R_2NO^- or changes in substituent groups on the cat^{2-} ligand.

Experimental Section

Physical Measurements. Equipment and procedures for cyclic voltammetry (CV), normal-pulse voltammetry (NPV) and controlled-potential coulometry (CPC) were the same as described previously[4] except that a Pt-gauze rather than a Pt-foil working electrode was used for CPC. Acetonitrile and dichloromethane distilled-in-glass solvents from Burdick & Jackson were stored over molecular sieves. Tetra-*n*-butylammonium hexafluorophosphate ($(TBA)PF_6$) supporting electrolyte from Southwestern Analytical Chemicals was vacuum-dried before use. Electrode potentials were measured against an aqueous saturated calomel electrode immersed in a 0.1 M $(TBA)PF_6/CH_3CN$ salt bridge but are reported against the ferrocene/ferrocenium (Fc^+/Fc) redox couple as described previously.[6] The $E^{\circ\prime}$ of the Fc^+/Fc couple in 0.1 M $(TBA)PF_6/CH_3CN$ was 0.386 ± 0.008 V vs SCE.

Infrared spectra were recorded on an IBM Series IR/98 Fourier transform spectrometer at 4-cm^{-1} resolution with a Happ-Genzel apodization function. All samples were run as KBr pellets (0.5-mg sample in 80 mg of KBr), and 500 spectra were signal averaged. Bands assigned to ν(Mo=O) are listed in Table I.

UV-visible spectra were recorded in distilled-in-glass CH_3CN on a Perkin-Elmer 552 spectrometer. Absorption maxima and molar absorptivities are presented in Table I.

^{95}Mo nuclear magnetic resonance spectra were obtained at the University of California at Davis Regional NMR facility on a Nicolet NT200 instrument operating at ca. 13 MHz and using the pulsed Fourier transform technique. Field homogeneity was adjusted by shimming on the ^{2}H resonance of a ^2H_2O-containing capillary within a 20-mm-o.d. tube of an aqueous 2 M $Na_2MoO_4 \cdot 2H_2O$ (pH 11) solution. Thereafter, spectra were recorded in the unlocked mode. Chemical shifts were referenced externally and are accurate to within ±1 ppm. Spectra were obtained at 295 K by using 20-mm-o.d. tubes containing about 15 mL of a ca. 0.1 M (or saturated) sample solution in acetonitrile, without sample rotation. Chemical shifts and line widths are listed in Table I.

Preparation of Compounds. *cis*-Dioxobis[hydroxylamido(1−)-*O*,*N*]molybdenum(VI), $[MoO_2(ONR_2)_2]$. These compounds were prepared for R = CH_3, C_2H_5, and $C_6H_5CH_2$ by variations on previously published syntheses.[7] For R = CH_3, addition of the hydrochloride of dimethylhydroxylamine to Na_2MoO_4 (2:1) in water was sufficient to cause precipitation of product in quantitative yield. For R = C_2H_5, 6 M hydrochloric acid was used to adjust the aqueous mixture of the free hydroxylamine with Na_2MoO_4 to pH 6 to cause quantitative product precipitation. Because dibenzylhydroxylamine is insoluble in water, a methathetical reaction of $MoO_2(acac)_2$ (acac = acetylacetonato) with $(C_6H_5CH_2)_2NOH$ (1:2) in hot methanol was used and gave quantitative precipitation of product.

[1,2-Benzenediolato(2−)-*O*,*O*′]oxobis[hydroxylamido(1−)-*O*,*N*]molybdenum(VI), $[MoO(X\text{-}cat)(ONR_2)_2]$. For R = CH_3 and C_2H_5 and X = H, 4-methyl, 4-nitro, and 3,5-di-*tert*-butyl, the preparative procedure used

(5) Bristow, S.; Enemark, J. H.; Garner, C. D.; Minelli, M.; Morris, G. A.; Ortega, R. B. *Inorg. Chem.* **1985**, *24*, 4070.
(6) Gagné, R. R.; Koval, C. A.; Lisensky, G. C. *Inorg. Chem.* **1980**, *19*, 2855.
(7) (a) Weighardt, K.; Holzbach, W.; Weiss, J.; Nuber, B.; Prikner, B. *Angew. Chem., Int. Ed. Engl.* **1979**, *18*, 548. (b) Weighardt, K.; Hofer, E.; Holzbach, W.; Nuber, B.; Weiss, J. *Inorg. Chem.* **1980**, *19*, 2927. (c) Weighardt, K.; Holzbach, W.; Hofer, E.; Weiss, J. *Inorg. Chem.* **1981**, *20*, 343. (d) Saussine, L.; Minmoun, H.; Mitschler, A.; Fischer, J. *Nouv. J. Chim.* **1980**, *4*, 235.

is exemplified by that for $MoO(C_6H_4O_2)[ON(C_2H_5)_2]_2$. Catechol (1.1 g, 10 mmol) was added to a solution of *cis*-$MoO_2[ON(C_2H_5)_2]_2$ (3.04 g, 10 mmol) in warm methanol (40 mL) to give an immediate deep red solution. The solution was stirred for 18 h. Water (100 mL) was added, the resulting mixture stirred for 30 min, and the crystalline precipitate filtered off. After the precipitate was washed copiously with water and dried under vacuum, the yield of $MoO(C_6H_4O_2)[ON(C_2H_5)_2]_2$ was 3.39 g (86%). The compound may be recrystallized from aqueous ethanol. With the 4-Me (74% yield) and 4-nitro (90% yield) derivatives, the crystalline precipitate was washed with cold methanol, followed by cold ether, and air dried.

For R = $C_6H_5CH_2$, similar reactions were carried out in 1:1 methanol/dichloromethane. For X = H, 4-CH_3, and 3,5-di-*tert*-butyl, equivalent quantities of the reactants were stirred in a stoppered flask for 3 days at room temperature. The crystalline product (~65% yield) was filtered off, washed with methanol and ether, and dried under vacuum. Additional product (~20% yield) was obtained on cooling the filtrate overnight at 4 °C. For X = 4-nitro, a similar equivalent reaction mixture was initially heated to boiling, then allowed to cool, and stirred overnight in a unstoppered flask. The crimson product (84% yield) was filtered off, washed with ether, and air dried.

Analytical and yield data are collected in Table I.

Results

Synthesis. 1,2-Dihydroxybenzene (catechol) and its derivatives (X-cat) react with *cis*-$MoO_2(ONR_2)_2$ to give the intensely red-to-violet, seven-coordinate compounds, $MoO(ONR_2)_2$(X-cat), as shown in eq 1. This reaction has previously been demonstrated

$$MoO_2(ONR_2)_2 + X\text{-}C_6H_3(OH)_2 \rightarrow MoO(ONR_2)_2(X\text{-}C_6H_3O_2) + H_2O \quad (1)$$

for *cis*-$MoO_2(S_2CNEt_2)_2$[4b] and *cis*-$MoO_2(ONC_5H_{10})_2$.[5] The visually determined rate of reaction depends on both R and X and increases in the order 4-CH_3 < 3,5-di-*tert*-butyl ~ H < 4-nitro for X and $C_6H_5CH_2 \ll CH_3 \sim C_2H_5$ for R. For reasonable reactions times to be achieved with R = $C_6H_5CH_2$, a mixed solvent system containing CH_2Cl_2 in addition to CH_3OH is used. Even so, several days are required for quantitative formation of $MoO[ON(CH_2C_6H_2)_2]_2(C_6H_4O_2)$ at ambient temperature. With the exception of some of the R = C_2H_5 derivatives, for which water was used as a precipitant, the majority of the products crystallize from the reaction mixtures in a highly pure form.

Spectroscopic Properties. The ^{95}Mo NMR spectra of each of the $MoO(ONR_2)_2$(X-cat) (R = CH_3, C_2H_5) complexes in acetonitrile show a single resonance with typical full widths at half-maximum of about 200–300 Hz (see Table I). The lines are at least twice as wide of those of the parent $MoO_2(ONR_2)_2$ compounds (ca. 110 Hz). As reported previously,[5] the Mo nuclei of these seven-coordinate, monooxocatecholato species are deshielded with respect to the dioxo parents, which have resonances at −165 ppm for R = CH_3 and at −173 ppm for R = C_2H_5, by about ca. 150 ppm. The extent of deshielding depends on the catecholato substituent and increases in the order 4-nitro < H < 4-methyl < 3,5-di-*tert*-butyl[8] as well as on the R group of the hydroxylamido ligand where $CH_3 < C_2H_5$ by 15–20 ppm. There is no indication in these spectra of the presence in solution of the two geometrical isomers of those compounds containing unsymmetric catecholates. Due to their low solubility, the ^{95}Mo NMR spectra of the dibenzylhydroxylamido compounds were not pursued.

The Fourier transform IR spectra of these compounds all show sharp, intense bands between ca. 930 and 915 cm^{-1}. These bands (see Table I) are assigned to the terminal molybdenum–oxygen stretching vibration, ν(Mo=O), by comparison with the spectra of the parent compounds and the free ligands and previously reported data.[5] For all three series of compounds, ν(Mo=O) decreases in energy with the X substituent on the catecholate in the order 4-nitro > H ~ CH_3 > 3,5-di-*tert*-butyl. For X = H and 4-CH_3, only a single, sharp, intense band at ca. 925 cm^{-1} is observable. For X = 3,5-di-*tert*-butyl, two clearly resolved, strong, approximately equally intense absorptions, at slightly lower energy, are observed. Although solid-state splittings could be responsible, assignment of both bands as ν(Mo=O) is preferred, one for each of the two geometric isomers possible for these compounds when unsymmetrical catecholate ligands are bound. These isomers are represented by structures I and II. Apparently, the *tert*-butyl groups in the 3- and 5-positions on the benzene ring produce sufficient steric interactions such that I and II have uniquely observable ν(Mo=O) stretches. In contrast, the single methyl group in the 4-position is insufficiently disruptive. Such geometric isomers have, however, been observed by ^{1}H and ^{13}C NMR spectroscopy.[5] For X = 4-nitro, a complex picture emerged. With $(C_2H_5)_2NO$ ligands, a single intense band at 931 cm^{-1} is the only band in this region not assignable to other ligands and so is the obvious candidate for ν(M=O). Its increased energy is consistent with the electron-withdrawing effect of the 4-nitro group, encouraging increased π-donation from O to Mo. However, with $(CH_3)_2NO$, two unique bands are observed at 929 (m, sh) and 922 (s) cm^{-1}, and with $(C_6H_5CH_2)_2NO$, three equally intense bands are observed at 937 (m), 929 (m), and 924 (m) cm^{-1}. Although no real distinction among these candidates for ν(M=O) can be made, possibly the band at 929 cm^{-1} in each compound may be preferred by comparison with that for the ethyl analogue.

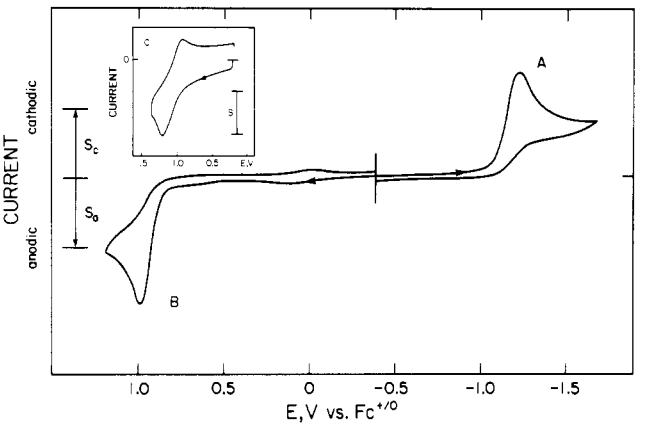

Figure 1. Cyclic voltammetry of $MoO(NO_2cat)_2(ONMe_2)_2$ in 0.1 M Bu_4NPF_6/CH_3CN at a 0.02 cm^2 Pt electrode: (A) voltammetric reduction, 1.28 mM complex, v = 0.05 V s^{-1}, S_c = 4 μA; (B) voltammetric oxidation as in part A, but with S_a = 10 μA; (C) fast-sweep-rate oxidation, 0.90 mM complex, v = 160 V s^{-1}, S = 200 μA.

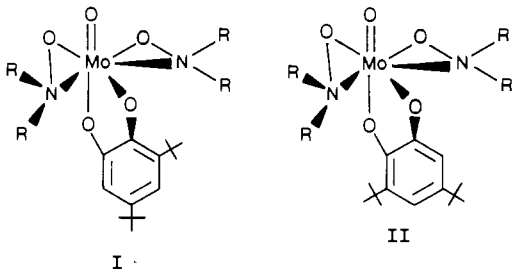

The UV–visible spectra of the $MoO(cat)(ONR_2)_2$ complexes each contain 2–3 absorption bands (Table I). The band at longest wavelength is similar in energy and intensity to a transition in the $MoO(cat)(S_2CNEt_2)_2$ complexes.[4b] On the basis of the d^0 electronic configuration of the metal, this transition is assigned to catechol-to-Mo charge transfer. The transition occurs at higher energies in the $MoO(cat)(ONR_2)_2$ complexes (λ_{max} = 457–542 nm) compared with $MoO(cat)(S_2CNEt_2)_2$ (λ = 509–572 nm) and, in both series of complexes, shifts to lower energy with more electron-donating catechol substituents.

Electrochemistry. Cyclic voltammetry, normal-pulse voltammetry, and controlled-potential coulometry were used to characterize the electrochemical behavior of the $MoO(cat)(ONR_2)_2$ complexes. Data obtained in CH_3CN are collected in Table II. Comparable results were obtained in CH_2Cl_2. The cyclic volt-

(8) A value of −28 ppm reported[5] for the chemical shift of the related complex $MoO(ONC_5H_{10})_2$(DTBcat) is incorrect. The correct result is +20 ppm: Enemark, J. H.; Garner, C. D.; Toohey, M., private communication.

Table II. Electrochemical Data for $MoO(X\text{-cat})(ONR_2)_2$ Complexes[a]

(a) Reductions

	CV			NPV		CPC	
	E_{pc}, V	$E_{pc} - E_{p/2}$, mV	$i_p/v^{1/2}AC$, $\mu A\ s^{1/2}\ V^{-1/2}\ cm^{-2}\ mM^{-1}$	$E_{1/2}$, V	i_d/AC, $\mu A\ cm^{-2}\ mM^{-1}$	E_{app}, V	n
$MoO(NO_2cat)(ONMe_2)_2$	−1.241	85	990	−1.21	1260	−1.4	1.33
$MoO(Cat)(ONMe_2)_2$	−1.455	120	830	−1.44	1250	−1.7	1.54
$MoO(CH_3cat)(ONMe_2)_2$	−1.517	110	1080	−1.62	1580	−1.7	1.44
$MoO(DTBcat)(ONMe_2)_2$	−1.545	133	820	−1.53	1160	−1.9	1.41
$MoO(NO_2cat)(ONEt_2)_2$	−1.303	70	650	−1.33	1610		
$MoO(Cat)(ONEt_2)_2$	−1.580	124	790	−1.55	1620		
$MoO(CH_3cat)(ONEt_2)_2$	−1.629	118	1030	−1.58	1370		
$MoO(DTBcat)(ONEt_2)_2$	−1.729	137	940	−1.62	1140		
$MoO(NO_2cat)(ONBz_2)_2$[b]	−1.118	98		−1.11			
$MoO(Cat)(ONBz_2)_2$[b]	−1.308	92		−1.30			
$MoO(CH_3cat)(ONBz_2)_2$[b]	−1.383						
$MoO(DTBcat)(ONBz_2)_2$[b]	−1.458	80		−1.48			

(b) Oxidations

	CV				NPV		CPC	
	E_{pa}, V	$E_{pa} - E_{p/2}$, mV	$E^{\circ\prime}$,[c] V	$i_p/v^{1/2}AC$, $\mu A\ s^{1/2}\ V^{-1/2}\ cm^{-2}\ mM^{-1}$	$E_{1/2}$, V	i_d/AC, $\mu A\ cm^{-2}\ mM^{-1}$	E_{app}, V	n
$MoO(NO_2cat)(ONMe_2)_2$	0.97	65	1.08	2820	0.96	4930		
$MoO(Cat)(ONMe_2)_2$	0.61, 0.75	59	0.66	2200	0.58, 0.78	4300		
$MoO(CH_3cat)(ONMe_2)_2$	0.54, 0.64	66	0.55	1700	0.53	1820		
$MoO(DTBcat)(ONMe_2)_2$	0.51	75	0.47	1350	0.48	1030	0.7	2.82
$MoO(NO_2cat)(ONEt_2)_2$	0.99	66	1.09	2140	1.00	2020		
$MoO(Cat)(ONEt_2)_2$	0.63	66	0.66	1700	0.62	1740		
$MoO(CH_3cat)(ONEt_2)_2$	0.55, 0.65	65	0.54	1690	0.52	1400		
$MoO(DTBcat)(ONEt_2)_2$	0.50	84	0.45	1220	0.46	1100	0.7	3.02
$MoO(NO_2cat)(ONBz_2)_2$[b]	1.03	63	1.20		1.12			
$MoO(Cat)(ONBz_2)_2$[b]	0.72	63	0.74		0.62			
$MoO(CH_3cat)(ONBz_2)_2$[b]	0.72		0.65					
$MoO(DTBcat)(ONBz_2)_2$[b]	0.61	85	0.60		0.52			

[a] Recorded in 0.1 M $(TBA)PF_6/CH_3CN$ at a 0.02 cm^2 Pt-disk electrode. Potential in V vs Fc^+/Fc. CV sweep rate = 0.05 V s^{-1} except as noted. [b] Insufficiently soluble for accurate determination of current parameter. [c] $E^{\circ\prime} = {}^1/_2(E_{pa} + E_{pc})$ for eq 3 by fast-sweep-rate CV (range of v = 0.2–280 V s^{-1}).

ammogram of $MoO(NO_2cat)(ONMe_2)_2$ in Figure 1 illustrates the electrochemical behavior.

Each complex exhibits a cathodic wave at negative potential (−1.1 to −1.7 V vs Fc^+/Fc), which is assigned to metal-centered reduction, and an anodic wave at positive potentials (0.5–1.0 V), which is assigned to oxidation of the coordinated catechol ligand. Neither of these waves is fully reversible at the sweep rates accessible to pen-and-ink recorders. However, as indicated by the inset to Figure 1, chemically reversible ligand-centered oxidation can be isolated by fast-sweep-rate CV. The metal-centered reduction remains irreversible under these conditions. The corresponding $MoO(cat)(S_2CNEt_2)_2$ complexes exhibit greater electrochemical reversibility.[4] For these latter complexes, all ligand-centered oxidations are reversible at moderate sweep rates (≤0.2 V s^{-1}), and the metal-centered reductions are chemically reversible for catecholate ligands with electron-withdrawing substituents.

The reductions of $MoO(cat)(ONR_2)_2$ exhibit peak currents that increase linearly with $v^{1/2}$ at sweep rates between 0.05 and 0.2 V s^{-1}, indicating that the electrode reactions are diffusion controlled. However, both the observed voltammetric peak widths ($E_{pc} - E_{p/2}$ = 70–140 mV) and the shifts in peak potential with sweep rate ($\Delta E_{pc}/\Delta(\log v)$ = 45–100 mV) are larger than the 57 and 30 mV values, respectively, associated with Nernstian one-electron transfer.[9] These data indicate that the metal-centered reductions are electrochemically irreversible. The cathodic cyclic voltammetric peak current parameters in Table II exhibit values appropriate to a one-electron transfer in CH_3CN.[10] However, the irreversibility of the electrode reaction means that $i_p/v^{1/2}AC$ is not a reliable indicator of the number of electrons transferred. We attempted a more reliable determination of this quantity by normal-pulse voltammetry and controlled-potential coulometry. A one-electron electrode reaction in CH_3CN exhibits an NPV current parameter of i_d/AC = 970 $\mu A\ cm^{-2}\ mM^{-1}$.[10] The cathodic i_d/AC values in Table II have a range of 1140–1620 $\mu A\ cm^{-2}\ mM^{-1}$. This result could reflect a larger diffusion coefficient for $MoO(cat)(ONR_2)_2$ species due to the relatively small size of the hydroxylamido ligand. However, controlled-potential coulometry yields $n = 1.4 \pm 0.1$ for reduction of the four $MoO(cat)(ONMe_2)_2$ complexes (Table II). Thus, we conclude that reduction of the $MoO(cat)(ONR_2)_2$ complexes proceeds by an irreversible one-electron transfer

$$Mo^{VI}O(cat)(ONR_2)_2 + e^- \rightarrow [Mo^{V}O(cat)(ONR_2)_2]^- \quad (2)$$

followed by chemical reactions that enhance the current at the potential of this wave by ~50%. Similar behavior is observed in the reduction of $MoO(cat)(S_2CNEt_2)_2$ complexes with electron-withdrawing catechol substituents, where chemical reactions following the initial electron transfer result in apparent electron stoichiometries of ~1.5 by NPV and CPC.[4a] Because of the irreversible nature of reaction 1, it is not possible to obtain further information about the chemical reactions that follow $MoO(cat)(ONR_2)_2$ reduction.

The anodic wave of the $MoO(cat)(ONR_2)_2$ complexes is assigned to oxidation of the bound catecholate ligand. The potential of this reaction is ca. 0.4 V more positive than the corresponding oxidation in $MoO(cat)(S_2CNEt_2)_2$ complexes and ca. 2.0 V more positive than $cat^{2-} \rightarrow SQ^{\bullet-}$ oxidation of the isolated ligands.[4b] Figure 1B shows that removal of an electron from $MoO(NO_2cat)(ONMe_2)_2$ is irreversible at 0.05 V s^{-1}. However, Figure 1C shows that this process becomes chemically reversible with i_{pc}/i_{pa} = 1.0 at a sweep rate of 160 V s^{-1}. Chemical reversibility increases with increasing electron-donor strength of the catechol

(9) Nicholson, R. S.; Shain, I. *Anal. Chem.* **1964**, *36*, 706.
(10) See Table I in ref 4a.

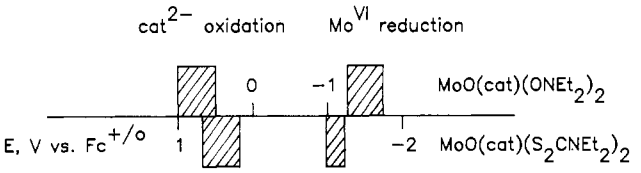

Figure 2. Range of redox potentials observed for $MoO(cat)(ONEt_2)_2$ and $MoO(cat)(S_2CNEt_2)_2$ complexes.

substituents. Thus, the oxidations of $MoO(DTBcat)(ONR_2)_2$ (R = Me,Et) exhibit a peak current ratio of $i_{pc}/i_{pa} = 0.8$ at 0.2 V s^{-1}. Chemically reversible behavior for the remaining $MoO(cat)(ONR_2)_2$ complexes was detected at sweep rates between these limits. Formal potentials ($E^{\circ\prime}$) for these oxidations, collected in Table II, are assigned to the electrode reaction

$$MoO(cat)(ONR_2)_2 \rightleftharpoons [MoO(SQ)(ONR_2)_2]^+ + e^- \quad (3)$$

For the $MoO(DTBcat)(ONR_2)_2$ (R = Me, Et) oxidations, reaction 3 is nearly reversible at moderate sweep rates, and the NPV and CV current parameters for this process agree with the value for a one-electron transfer in CH_3CN (Table II). The current parameters are much larger for the remaining oxidations. In addition, coulometric oxidation of $MoO(DTBcat)(ONMe_2)_2$ and $MoO(DTBcat)(ONEt_2)_2$ at potentials slightly positive of $E^{\circ\prime}$ yields $n \simeq 3$. We attribute this behavior to chemical reactions involving the oxidized catechol moiety, which lead to transfer of additional electrons. Extensive reactivity of a similar nature occurs during electrochemical oxidation of uncomplexed catechols.[11] The chemical reactivity of the semiquinone is much greater when coordinated to the $MoO(ONR_2)_2^{2+}$ center than to the corresponding $MoO(S_2CNEt_2)_2^{2+}$ unit. In the latter case, fully reversible behavior is observed for the electrode reaction

$$MoO(cat)(S_2CNEt_2)_2 \rightleftharpoons [MoO(SQ)(S_2CNEt_2)_2]^+ + e^- \quad (4)$$

with eight different catecholate ligands. Also, solutions of $[MoO(DTBSQ)(S_2CNEt_2)_2]^+$ in CH_2Cl_2 are stable for many hours and exhibit an EPR spectrum consistent with Mo–semiquinone coordination.[4b]

It should be noted that different reasons are responsible for the irreversible character of the ligand- and metal-centered electrode reactions of $MoO(cat)(ONR_2)_2$ complexes. The voltammetric peak widths and peak potential shifts with sweep rate for the ligand-centered oxidation (eq 3) are $E_{pa} - E_{p/2} = 65 \pm 5$ mV and $\Delta E_{pa}/\Delta(\log v) = 28 \pm 2$ mV, respectively. These values indicate reversible electron transfer followed by an irreversible chemical reaction,[9] consistent with the chemical reactivity of electrogenerated $[MoO(SQ)(ONR_2)_2]^+$ described above. The irreversibility of the metal-centered reductions (eq 2) is associated with the electron-transfer step itself. Here, $E_{pc} - E_{p/2} = 70$–140 mV and $\Delta E_{pc}/\Delta(\log v) = 45$–$110$ mV. In the reduction of $MoO(cat)(S_2CNEt_2)_2$ complexes, we identified[4c] this irreversibility as deriving from large reorganization energy barriers, i.e., changes in the nuclear coordinates of ligand donor atoms, that must be overcome in transferring an electron to the metal. Similar conditions apparently prevail in reduction of the $MoO(cat)(ONR_2)_2$ complexes. By comparison, much smaller reorganizational barriers accompany electron abstraction from the coordinated catecholate ligand.

Discussion

Redox Potentials. The range of redox potentials exhibited by $MoO(cat)(ONEt_2)_2$ and $MoO(cat)(S_2CNEt_2)_2$ complexes is illustrated in Figure 2. The width of the bars indicates the range of values observed between 4-nitro- and 3,5-di-*tert*-butylcatecholate derivatives. The potentials for metal-centered reductions and ligand-centered oxidations shift in the negative direction with catechol X-substituent in the sequence 4-nitro < H < 4-CH_3 < 3,5-di-*tert*-butyl as expected from the electron-donor/electron acceptor properties of these groups. Also, metal-centered reductions of the $MoO(cat)(ONEt_2)_2$ complexes are observed at potentials more negative than those for reductions of the corresponding $MoO(cat)(S_2CNEt_2)_2$ complexes in consonance with the greater electron-donor strength of hydroxylamide vs dithiocarbamate ligand. However, the corollary expectation regarding ligand-centered oxidations is not realized; these occur at *more positive* potentials for $MoO(cat)(ONEt_2)_2$. Thus, the $MoO(cat)(ONEt_2)_2$ complexes exhibit a greater difference in energy between the potentials of Mo(VI) reduction and catecholate oxidation than do the corresponding $MoO(cat)(S_2CNEt_2)_2$ complexes. Explanation of this observation is provided following consideration of other properties of these compounds.

Correlation of Optical and Electrochemical Properties. Each of the $MoO(cat)(ONR_2)_2$ and $MoO(cat)(S_2CNEt_2)_2$ complexes exhibits an intense visible wavelength absorption band assigned to ligand-to-metal charge transfer.

$$Mo^{VI}O(cat)L_2 \xrightarrow[LMCT]{h\nu} [Mo^{V}O(SQ)L_2]^* \quad (5)$$

$$L = R_2NO^-,\ Et_2NCS_2^-$$

There is continuing interest[12-18] in relationships between electrochemical and spectroscopic properties, and we have attempted to correlate these charge transfer energies ($h\nu_{ct}$) with differences between metal- and ligand-centered redox potentials (ΔE_{redox}) for compounds of both types. For the intramolecular charge transfer in eq 5, ΔE_{redox} is the difference between the potential for oxidation of the ligand (eq 6) and that for reduction of the metal (eq 7).

$$[Mo^{VI}\text{–cat}] \rightarrow [Mo^{VI}\text{–SQ}]^+ + e^- \quad E_{cat}^{ox} \quad (6)$$

$$[Mo^{VI}\text{–SQ}]^+ + e^- \rightarrow [Mo^{V}\text{–SQ}] \quad E_{Mo}^{red'} \quad (7)$$

However, the potential of eq 7 cannot be determined experimentally because coordinated $SQ^{\bullet-}$ is reduced before Mo(VI). Thus, it is necessary to substitute for $E_{Mo}^{red'}$ the potential of reaction 8

$$[Mo^{VI}cat] + e^- \rightarrow [Mo^{V}cat]^- \quad E_{Mo}^{red} \quad (8)$$

and to carry out the correlation using the relationship

$$h\nu_{ct} = a(\Delta E_{redox}) + \text{constant} \quad (9)$$

where $\Delta E_{redox} = E_{cat}^{ox} - E_{Mo}^{red}$. For E_{cat}^{ox}, we use the $E^{\circ\prime}$ of the reversible ligand-centered oxidation (eq 3), and for E_{Mo}^{red}, $E_{pc/2}$, the voltammetric half-peak potential for metal-centered reduction (eq 2) evaluated at a sweep rate of 0.05 V s^{-1}, is used. Data are taken from Tables I and II for the $MoO(cat)(ONR_2)_2$ compounds and from previously unpublished results (Table III, supplementary material) for the $MoO(cat)(S_2CNEt_2)_2$ compounds. It should be noted that $E_{pc/2}$ corresponds to an irreversible electrode reaction for many of the compounds considered. Use of this term is justified because the shifts in $E_{pc/2}$ with ligand substituent group are similar in direction and magnitude to the shift in $E^{\circ\prime}$ of a reversible

(11) Ryan, M. D.; Yueh, A.; Chen, W.-Y. *J. Electrochem. Soc.* **1980**, *127*, 1489.

(12) (a) Vlcek, A. A. *Electrochim. Acta* **1968**, *13*, 1063. (b) Peover, M. E. *Electrochim. Acta* **1968**, *13*, 1083.

(13) (a) Saji, T.; Aoyagui, S. *J. Electroanal. Chem. Interfacial Electrochem.* **1975**, *60*, 1. (b) Saji, T.; Aoyagui, S. *J. Electroanal. Chem. Interfacial Electrochem.* **1975**, *63*, 405.

(14) (a) Curtis, J. C.; Sullivan, B. P.; Meyer, T. J. *Inorg. Chem.* **1983**, *22*, 224. (b) Kober, E. M.; Sullivan, B. P.; Meyer, T. J. *Inorg. Chem.* **1984**, *23*, 2098.

(15) (a) Goswami, S.; Mukherjee, R.; Chakravorty, A. *Inorg. Chem.* **1983**, *22*, 2825. (b) Ghosh, P.; Chakravorty, A. *Inorg. Chem.* **1984**, *23*, 2242.

(16) Ohsawa, Y.; Hanck, K. W.; DeArmond, M. K. *J. Electroanal. Chem. Interfacial Electrochem.* **1984**, *175*, 229.

(17) (a) Dodsworth, E. S.; Lever, A. B. P. *Chem. Phys. Lett.* **1984**, *112*, 567. (b) Dodsworth, E. S.; Lever, A. B. P. *Chem. Phys. Lett.* **1985**, *119*, 61. (c) Dodsworth, E. S.; Lever, A. B. P. *Chem. Phys. Lett.* **1986**, *124*, 152. (d) Haga, M.-A.; Dodsworth, E. S.; Lever, A. B. P. *Inorg. Chem.* **1986**, *25*, 447.

(18) Lever, A. B. P. *Inorganic Electronic Spectroscopy*, 2nd ed.; Elsevier: Amsterdam, 1984.

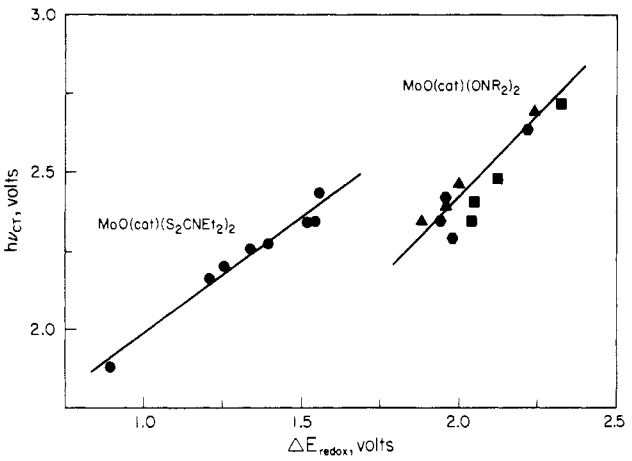

Figure 3. Plot of ligand-to-metal charge-transfer energies vs difference between ligand- and metal-centered redox potentials for MoO(cat)(S_2CNEt_2)$_2$ (●) and MoO(cat)(ONR_2)$_2$ [(▲) R = Me; (■) R = Et; (●) R = Bz] complexes.

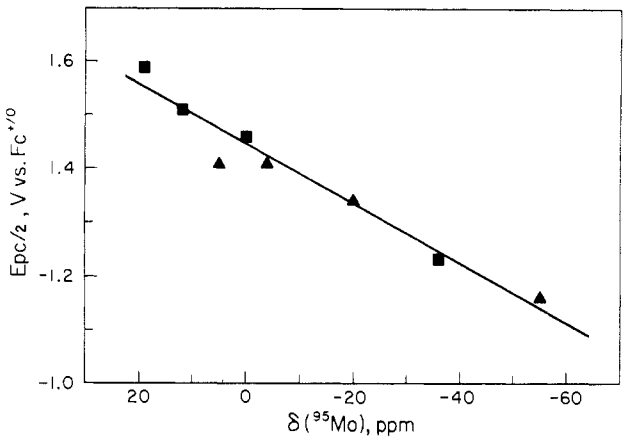

Figure 4. Plot of voltammetric half-peak potential vs ^{95}Mo chemical shift for MoO(cat)(ONR_2)$_2$ complexes [(▲) R = Me; (■) R = Et].

electrode reaction.[19] Furthermore, five of the eight MoO(cat)(S_2CNEt_2)$_2$ complexes exhibit quasi-reversible metal-centered electron transfer in CH_3CN (Table III, supplementary material). In these cases, $(E^{\circ\prime} - E_{pc/2}) \leq 0.02$ V, indicating that $E_{pc/2}$ is a good estimate of the thermodynamic $E^{\circ\prime}$.

Plots of $h\nu_{ct}$ vs ΔE_{redox} in acetonitrile are shown in Figure 3. Linear regression analysis yields $h\nu_{ct} = 0.74(\Delta E_{redox}) + 1.25$ ($r = 0.981$) for the MoO(cat)(S_2CNEt_2)$_2$ complexes and $h\nu_{ct} = 0.96(\Delta E_{redox}) + 0.48$ ($r = 0.916$) for the MoO(cat)(ONR_2)$_2$ complexes. Separate correlation lines are observed for the two families of compounds. The slope of the MoO(cat)(S_2CNEt_2)$_2$ line is significantly less than unity, and the vertical offset between the lines is ca. 0.8 V. If the two lines are translated either vertically or horizontally, it is apparent that the R_2NO^- complexes have larger values of $h\nu_{ct}$ and ΔE_{redox} than the $Et_2NCS_2^-$ species as suggested by Figure 2. A remarkable feature of Figure 3 is the large effect of coligand on the charge-transfer and redox energetics of the MoO^{4+}–catecholate center. To our knowledge, an effect of this magnitude has not been demonstrated before. It is noticeably absent, for example, in correlations involving the Ru(II) → bpy (π^*) transitions of $[Ru(bpy)_2XY]^{n+}$ ($n = 0, 1, 2$) complexes.[17c]

Better understanding of possible reasons for nonunit slope and the large offset between correlation lines can be gained from a more detailed analysis of charge-transfer and redox relationships. We adopt the approach of Dodsworth and Lever for this purpose.[17,21] Their result is

$$h\nu_{ct} = \Delta E_{redox} + Y + \chi_i + \chi_o \qquad (10)$$

where $Y = E_{Mo}^{red} - E_{Mo}^{red'}$ and χ_i and χ_o are the inner- and outer-sphere reorganization energies associated with the electronic transition. A slope of less than 1 for eq 9 indicates that one or more of the terms $Y + \chi_i + \chi_o$ in eq 10 contains an implicit dependence on ΔE_{redox}. The MoO(cat)(S_2CNEt_2)$_2$ complexes exhibit such behavior, but it is not possible to extract the source of this dependence from the data available.

Offset between the two correlation lines results from differences in terms on the rhs of eq 10. The quantity Y accounts for the fact that eq 7 rather than eq 8 should be used to calculate the energy difference between ground and excited states of the spectroscopic transition. Y cannot be determined experimentally, but its magnitude can be estimated by comparing formal potentials of the $MoO(S_2CNEt_2)_3^{+/0}$ couple (−0.7 V vs Fc^+/Fc)[4a] and the chemically reversible $[MoO(cat)(S_2CNEt_2)_2]^{0/-}$ couples (Table III), which span the range $E^{\circ\prime} = -0.8$ to −1.0 V. Thus, an increment of one unit of negative charge in the ligands surrounding the MoO^{4+} center accounts for a shift of 0.1–0.3 V in its redox potential. Given this small estimated magnitude of Y, it is unlikely that *differences* in this quantity could account for the observed offset. Also, large differences in the solvent reorganization term, χ_o, are not expected for the structurally similar MoO(cat)(ONR_2)$_2$ and MoO(cat)(S_2CNEt_2)$_2$ complexes. Therefore, ΔE_{redox} and χ_i are likely to be the largest contributors to the offset. ΔE_{redox} was calculated by using the voltammetric half-peak rather than formal potentials for E_{Mo}^{red}. Differences between $E_{pc/2}$ and $E^{\circ\prime}$ are small for the nearly reversible MoO(cat)(S_2CNEt_2)$_2$ reductions (Table III). However, the completely irreversible MoO(cat)(ONR_2)$_2$ reductions would be expected to exhibit larger differences between $E_{pc/2}$ and $E^{\circ\prime}$. This greater irreversibility is attributed to large inner-shell reorganization barriers accompanying electron transfer at the metal center (vide supra). This same factor presumably results in larger spectroscopic inner-shell reorganization energies, χ_i, for the hydroxylamido complexes. Thus, differences in both ΔE_{redox} and χ_i resulting from this property offer the best explanation for the offset between correlation lines in Figure 3.

Correlations with NMR Data. There have been relatively few attempts to correlate electrochemical and NMR spectroscopic data,[22-26] particularly when the nucleus for which the NMR chemical shift is measured is also the site of electron transfer.[22,25a,c] Having generated a data set containing metal-centered redox potentials and ^{95}Mo NMR chemical shifts for MoO(cat)(ONR_2)$_2$ (R = Me, Et) complexes, we sought to establish the existence of and reasons for relationships between these parameters. Figure 4 shows that a linear correlation exists between $E_{pc/2}$ and $\delta(^{95}Mo)$. However, the electrochemical potentials move to more negative values (in response to the electron-donor strength of the catechol substituents) as the ^{95}Mo chemical shifts become more deshielded.

(19) Use of irreversible $E_{pc/2}$'s in place of reversible E°'s is equivalent to subtituting kinetic for thermodynamic electrode parameters. Parameters of these two types generally respond in a parallel manner and to similar extents to changes in molecular structure.[20]

(20) (a) Klingler, R. J.; Kochi, J. K. *J. Am. Chem. Soc.* **1980**, *102*, 4790. (b) Faure, D.; Lexa, D.; Saveant, J. M. *J. Electroanal. Chem. Interfacial Electrochem.* **1982**, *140*, 285. (c) Andrieux, C. P.; Gallardo, I.; Saveant, J. M.; Su, K.-B. *J. Am. Chem. Soc.* **1986**, *108*, 638.

(21) Similar treatments are available in ref 14a and 16.

(22) Mayer, U.; Kotocova, A.; Gutmann, V.; Gerger, W. *J. Electroanal. Chem. Interfacial Electrochem.* **1979**, *100*, 875.

(23) Nesmeyanov, A. N.; Aleksanyan, V. T.; Denisovich, L. I.; Nekrasov, Yu. S., Fedin, E. I.; Khvostenko, V. I.; Kritskaya, I. I. *J. Organomet. Chem.* **1979**, *172*, 133.

(24) Nishida, Y.; Kida, S.; Cremer, S.; Nakamato, K. *Inorg. Chim. Acta* **1981**, *49*, 85.

(25) (a) Bond, A. M.; Colton, R.; Dakternieks, D.; Hanck, K. W. *Inorg. Chem.* **1982**, *21*, 117. (b) Bond, A. M.; Carr, S. W.; Colton, R.; Kelly, D. P. *Inorg. Chem.* **1983**, *22*, 989. (c) Bond, A. M.; Carr, S. W., Colton, R. *Organometallics* **1984**, *3*, 541.

(26) Davies, J. A.; Uma, V.; Mierzwiak, J. G. *J. Electroanal. Chem. Interfacial Electrochem.* **1985**, *196*, 329.

(27) (a) Harris, R. K., Mann, B. E., Eds. *NMR and the Periodic Table*; Academic: London, 1977. (b) Webb, G. A. In *NMR of Newly Accessible Nuclei*; Laszlo, P., Ed.; Academic: New York, 1983; Volume I, Chapter 4. (c) Minelli, M.; Enemark, J. H.; Brownlee, R. T. C.; O'Connor, M. J.; Wedd, A. G. *Coord. Chem. Rev.* **1985**, *65*, 169.

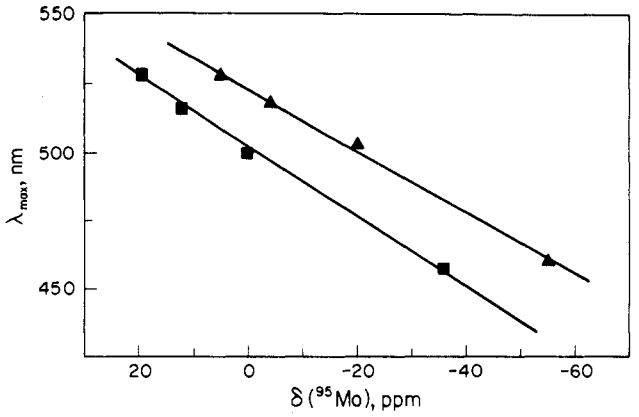

Figure 5. Plot of LMCT wavelength vs ^{95}Mo chemical shift for MoO(cat)$(ONR_2)_2$ complexes [(▲) R = Me; (■) R = Et].

This result is contrary to intuition, because an increase in electron density on Mo would be expected to lead to greater shielding of this nucleus.

The apparent anomaly is removed by consideration of the factors which contribute to the ^{95}Mo chemical shift. The shielding, σ, of heavy nuclei[27] results primarily from a sum of localized diamagnetic

$$\sigma_A^d(\text{loc}) = \left(\frac{\mu_0 e^2}{12\pi m}\right)\sum_B^A P_{uu}\langle u|1/r_A|u\rangle \qquad (11)$$

and paramagnetic terms

$$\sigma_A^p(\text{loc}) = \left(\frac{-\mu_0 e^2 h^2}{6\pi m^2 \Delta E_{exc}}\right)[\langle 1/r^3\rangle_p P_u + \langle 1/r^3\rangle_d D_u] \qquad (12)$$

In eq 11, P_{uu} is the charge density in atomic orbital u that is distance r_A from nucleus A. In eq 12, the term in brackets represents the anisotropy of the electric field about nucleus A arising from imbalance in its p and d orbital occupancy and ΔE_{exc} represents an average excitation energy of excited electronic states. σ_A^d(loc) is a ground-state term, whose major contribution derives from shielding by inner-shell electrons. Outer-shell and ligand donor atom electrons, which are associated with coordinate bonding effects, make only a small contribution to this term.[28] The paramagnetic term, σ_A^p(loc), involves mixing of ground and excited states in the applied magnetic field and, for heavy nuclei, is the principal contributor to σ. The electric field anisotropy would be expected to be relatively constant for the MoO(cat)$(ONR_2)_2$ complexes considered; thus, we would expect σ_A^p(loc) to vary as $1/\Delta E_{exc}$. If mixing with the lowest lying excited state only is considered, a linear relationship between chemical shift and the wavelength of LMCT (eq 5) should prevail (see eq 13). Figure

$$\sigma \simeq \sigma_A^p(\text{loc}) = -a\lambda_{max} \qquad (13)$$

5 shows excellent straight-line plots of $\delta(^{95}\text{Mo})$ vs λ_{max} for the MoO(cat)$(ONMe_2)_2$ and MoO(cat)$(ONEt_2)_2$ complexes. The existence of two correlation lines is not understood, but could reflect a small difference in the diamagnetic term arising from the different hydroxylamide substituent. The trend of the data in Figure 5 is in the expected direction for control of the chemical shift by σ_A^p(loc). Complexes with lower energy transitions are more deshielded because of the greater accessibility of the charge-transfer excited state. Similar correlations have been demonstrated for ^{59}Co,[29] ^{95}Mo,[30] and ^{183}W[30,31] nuclei. Analysis

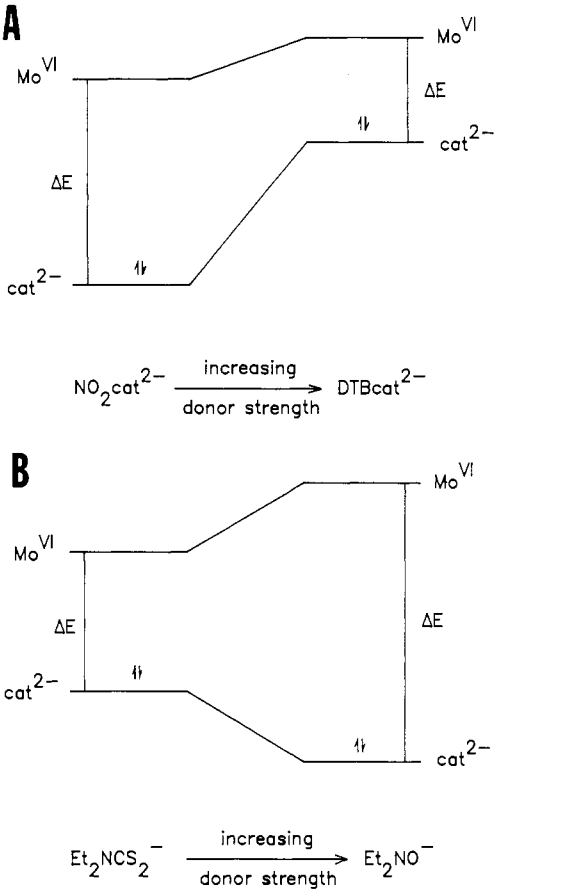

Figure 6. Response of Mo(VI) and catecholate orbital energies in MoO(cat)(L-L)$_2$ complexes to changes in (A) catechol substituent group and (B) L-L coligand.

of chemical shifts in terms of eq 10–13 also prompts the realization that the correlation between $E_{pc/2}$ and $\delta(^{95}\text{Mo})$ in Figure 4 is either fortuitous or indirectly derived through interpendence of the optical and electrochemical parameters.

Conclusions. In this work, we have demonstrated that the electrochemical, optical and NMR spectroscopic properties of MoO(cat)(L-L)$_2$ complexes respond to alterations in molecular structure involving changes in the L-L coligand and in the catechol substituent group. A basis for understanding the effects of these structural changes on electrochemical and spectroscopic properties can be obtained from the qualitative energy level diagrams shown in Figure 6.

Figure 6A shows the effect of changing the catechol substituent on the energies of the filled catecholate and vacant Mo(VI) orbitals. Both orbitals increase in energy with increasing donor strength of the substituent. This observation is consistent with the shifts of both redox potentials to more negative values indicating more difficult reduction of Mo(VI) and more facile oxidation of cat^{2-}. Since the substituent is attached directly to catechol, the catechol orbital experiences a greater change in energy. Thus, the difference between Mo and cat^{2-} levels decreases with increasing donor strength, which results in a smaller ΔE_{redox}, a lower charge-transfer energy and a more deshielded ^{95}Mo NMR chemical shift (as a result of its dependence on λ_{max}). All of these expectations are observed experimentally.

Figure 6B shows the effect of replacing the dithiocarbamate coligand with hydroxylamide. As R_2NO^- is more electron-donating than $Et_2NCS_2^-$, the metal-centered orbital should be raised in energy. Indeed, a more negative E_{pc} is observed for Mo(VI) reduction in response to this change. However, the catecholate orbital is stabilized, i.e., lowered in energy, by this interaction as indicated by more positive potentials for cat^{2-} → SQ$^{\bullet-}$ oxidation in the MoO(cat)$(ONR_2)_2$ complexes. Thus, there is a larger spacing between the Mo(VI) and cat^{2-} orbitals, which results in larger values of ΔE_{redox} and larger charge-transfer energies for

(28) (a) Nakatsuji, H.; Kanda, K.; Endo, K.; Yonezawa, T. *J. Am. Chem. Soc.* **1984**, *106*, 4653. (b) Kanda, K.; Nakatsuji, H.; Yonezawa, T. *J. Am. Chem. Soc.* **1984**, *106*, 5888.
(29) (a) Griffith, J. S.; Orgel, L. E. *Trans. Faraday Soc.* **1957**, *53*, 601. (b) Juranic, N.; Celap, M. B.; Vucelic, D.; Malinar, M. J.; Radivojsa, P. N. *J. Magn. Reson.* **1979**, *35*, 319.
(30) Gheller, S. F. Ph.D. Thesis, La Trobe University, 1985.
(31) Acerete, R.; Hammer, C. F.; Baker, L. C. W. *J. Am. Chem. Soc.* **1982**, *104*, 5384.

the $MoO(cat)(ONR_2)_2$ complexes. Both effects are observed experimentally (Figure 3).

An important implication of the results depicted in Figure 6 is that the variation in electronic properties of the molecules is qualitatively different for molecular structural changes made on the periphery of the ligands vs those made at the metal. In the former case, electronic effects are transmitted through the ligand to the metal with the result that both orbital energies change in the same direction, but with some diminution of the effect at the metal. However, when a change in the metal–coligand bond is made, the metal and catecholate orbital energies change in opposite directions. The result is increased stabilization of the filled catecholate (bonding) orbitals and decreased stabilization of the vacant molybdenum (antibonding) orbitals. Such changes are characteristic of interactions resulting from a chemical bonding process. They can be rationalized, for example, in terms of the theory of hard and soft acids and bases.[32] A change from soft $Et_2NCS_2^-$ to hard Et_2NO^- results in a larger HOMO/LUMO gap and predictable changes in the electrochemical and charge-transfer properties of the molecules.

(32) (a) Parr, R. G.; Pearson, R. G. *J. Am. Chem. Soc.* **1983**, *105*, 7512. (b) Pearson, R. G. *J. Am. Chem. Soc.* **1985**, *107*, 6801.

Acknowledgment. This study is dedicated to the memory of Professor Maxwell J. O'Connor, who initiated the interest of S.F.G. in this research area through example and encouragement. Support of this research by the National Science Foundation (F.A.S., Grant CHE-84-09594) is gratefully acknowledged. L.P.M. was an NSF Research Opportunity Award Participant at Florida Atlantic University, 1985. We thank S. Kint for the FT/IR spectra.

Registry No. I (R = Me), 111159-51-4; I (R = Et), 111159-52-5; I (R = Bz), 111159-54-7; II (R = Me), 111264-40-5; II (R = Et), 111264-37-0; II (R = Bz), 111264-38-1; $MoO(cat)(ONMe_2)_2$, 111159-49-0; $MoO(cat)(ONEt_2)_2$, 111188-97-7; $MoO(cat)(ONBz_2)_2$, 111159-53-6; $MoO(CH_3cat)(ONMe_2)_2$, 111159-55-8; $MoO(CH_3cat)(ONEt_2)_2$, 111159-57-0; $MoO(CH_3cat)(ONBz_2)_2$, 111159-59-2; $MoO(NO_2cat)(ONMe_2)_2$, isomer 1, 111159-50-3; $MoO(NO_2cat)(ONMe_2)_2$, isomer 2, 111264-39-2; $MoO(NO_2cat)(ONEt_2)_2$, 111159-56-9; $MoO(NO_2cat)(ONBz_2)_2$, 111159-58-1; *cis*-$MoO_2(ONMe_2)_2$, 74081-85-9; *cis*-$MoO_2(ONEt_2)_2$, 74081-86-0; *cis*-$MoO_2(ONBz_2)_2$, 74081-87-1; ^{95}Mo, 14392-17-7.

Supplementary Material Available: Table III, listing electrochemical and UV–visible properties of eight $MoO(cat)(S_2CNEt_2)_2$ complexes in acetonitrile (1 page). Ordering information is given on any current masthead page.

Contribution from the Department of Chemistry, Emory University, Atlanta, Georgia 30322, and Biophysics Laboratory and Molecular Pharmacology Laboratory, Division of Biochemistry and Biophysics, Food and Drug Administration, Bethesda, Maryland 20892

HMQC and ^1H and ^{31}P NMR Studies of Platinum Amine Adducts of Tetradeoxyribonucleotides. Relationship between ^{31}P Shift and Potential Hydrogen-Bonding Interactions in pGpG Moieties Cross-Linked by Platinum

Christine Spellmeyer Fouts,[†] Luigi G. Marzilli,*[†] R. Andrew Byrd,[‡] Michael F. Summers,[‡§] Gerald Zon,[‡∥] and Kazuo Shinozuka[‡]

Received December 24, 1986

The dependence of the ^{31}P and ^1H NMR spectra of d(TGGT) on formation of Pt adducts was studied with *cis*-PtA_2Cl_2 compounds, where A_2 = en, $(NH_3)_2$, $(MeNH_2)_2$, tn, Me_2tn, and *N,N*-Me_2en. In addition, more limited spectral studies were performed with the following oligonucleotides: d(TTGG), d(GGTT), and d(pGGTT). For all combinations studied, a downfield-shifted ^{31}P signal was observed after treatment with *cis*-PtA_2Cl_2. For d(TGGT)Pt(en) and d(TGGT)-*cis*-$Pt(MeNH_2)_2$, various 2D NMR techniques were selectively employed (NOE, HMQC, HOHAHA, and COSY). For d(TGGT)Pt(en), ^{17}O-labeling studies and 2D NMR methods assigned the downfield ^{31}P NMR signal to GpG, and NOE studies demonstrated that the Pt formed an intrastrand cross-link with the GpG moiety where the G residues were in a head-to-head configuration. 2D NMR methods led to these same conclusions with d(TGGT)-*cis*-$Pt(MeNH_2)_2$. For d(TGGT)Pt(en), the 3′-T was stacked with the 3′-G as evidenced by internucleotide NOEs. There was no indication of such stacking in d(TGGT)-*cis*-$Pt(MeNH_2)_2$. Nevertheless, by a combination of HMQC, HOHAHA, and COSY 2D NMR techniques, we were able to assign completely the ^1H NMR signals for d(TGGT)-*cis*-$Pt(MeNH_2)_2$; this example illustrates the power of the newer 2D methods in signal assignments. The downfield-shifted ^{31}P NMR signal appears to be characteristic of the intrastrand GG cross-link, and no such signal was observed in preliminary studies when the reactants [d(TGGT) + *trans*-$Pt(NH_3)_2Cl_2$] could not form such an adjacent GG cross-link. In contrast, ^1H NMR spectra revealed downfield ^1H signals for the d(TGGT) + *trans*-$Pt(NH_3)_2Cl_2$. Likewise, the shift of the downfield ^{31}P NMR signals of the GpG moiety can be correlated with the potential H-bonding ability of the Pt moiety and of the oligonucleotide. In particular, if there is a phosphate group 5′ to the GpG unit, the ^{31}P NMR signal is further downfield than in analogous species lacking such a group. Furthermore, when the amine group coordinated cis to the 5′-G is capable of H bonding (e.g. NH_2), the GpG ^{31}P signal is further downfield than when this group is cis to amines incapable of H bonding (e.g. Me_2N). Thus, the shift data are consistent with molecular mechanics calculations and recent X-ray structures, which indicate that the 5′-phosphate groups participate in H bonding. A simple correlation between ^1H NMR shifts of the G H8 signals and such H-bonding possibilities was not evident. Temperature and pH variation studies were also performed in selected cases. It is interesting that the downfield ^{31}P NMR signal of the GpG cross-linked moiety was relatively insensitive to such changes whereas ^1H NMR signals were often found to be quite sensitive, in agreement with literature studies.

Introduction

The antitumor agent *cis*-$Pt(NH_3)_2Cl_2$ is one of the most widely used anticancer drugs in the U.S.[1] Considerable evidence indicates that the primary molecular target of the drug is DNA[2] (see footnote 3 for abbreviations) and that the principal type of

[†] Emory University.
[‡] Food and Drug Administration.
[§] Current address: Department of Chemistry, University of Maryland, Baltimore County, Baltimore, MD 21228.
[∥] Current address: Applied Biosystems, Foster City, CA 94404.

(1) (a) Sun, M. *Science (Washington, D.C.)* **1983**, *222*, 145. See also: *Platinum Met. Rev.* **1984**, *28*, 157. (b) Pinto, A. L.; Lippard, S. J. *Biochim. Biophys. Acta* **1985**, *780*, 167.
(2) Roberts, J. J. In *Advances in Inorganic Biochemistry*; Eichhorn, G. L., Marzilli, L. G., Eds.; Elsevier North Holland: New York, 1981; Vol. 3, p 273.

0020-1669/88/1327-0366$01.50/0